Bulletin of the JSME Vol.17, No.2, 2023
Journal of Advanced Mechanical Design, Systems, and Manufacturing

Mobile parallel manipulator consisting of two nonholonomic carts and their path planning

Qiang YAO*, Tatsuro TERAKAWA*, Yuya MORITA* and Masaharu KOMORI*
*Department of Mechanical Engineering and Science, Kyoto University
Kyotodaigakukatsura, Nishikyo-ku, Kyoto-shi, Kyoto 615-8540, Japan
E-mail: terakawa@me.kyoto-u.ac.jp

Received: 11 July 2022; Revised: 23 October 2022; Accepted: 6 January 2023

Abstract
Mobile manipulators are widely used to transport and manipulate objects in industrial settings. In this paper, we propose a mobile manipulator that consists of a parallel mechanism and two two-wheel-drive carts. The planar motions of the carts are transmitted to a platform through three screw pairs of the parallel mechanism, allowing the pose of the platform to be controlled by only four motors. Kinematic analysis for such a two-cart mobile manipulator gives a Jacobian matrix, reveals the effects of nonholonomic constraints, and demonstrates that the yaw angle of the platform must be limited to avoid singular and failure configurations, and that the pitch angle is quite sensitive to uncertainties. Based on these analysis results, we present a custom path planning method for the carts. This method provides a non-optimal but easily realizable path planning algorithm with low computational cost, since the complex constraint conditions of this two-cart mobile manipulator have little influence on the proposed path generation process. The path planning process consists of four steps. We describe the motions of the carts in each step and establish a path tracking control system for the carts. Some simulations are conducted to show the motions of the carts, investigate the changes in the pose of the platform, and quantitatively evaluate the sensitivity of the platform's pitch angle. Moreover, we construct an experimental prototype and conduct experiments to verify the validity and usefulness of the proposed mechanism and path planning method.

Keywords : Mobile manipulator, Nonholonomic robot, Parallel mechanism, Path planning, Robot kinematics

1. Introduction

Manipulators mounted on mobile robots have been widely used in factories and warehouses because they have a high degree of freedom (DOF) and a wide working range (Arai, 1995). Mobile robots equipped with an open-loop manipulator [see Fig. 1(a)] have been developed (Yamamoto and Yun, 1992; Minami, et al., 1993; Jain and Kemp, 2009; Bischoff, et al., 2011). Closed-loop mechanisms have higher positioning accuracy and stiffness, and thus mobile robots with a closed-loop manipulator [see Fig. 1(b)], named mobile parallel manipulators (MPMs), have been studied. Various closed-loop mechanisms, such as Stewart platform (Stewart, 1965) and DELTA manipulators (Li, et al., 2006), have been fixed on a mobile base to develop MPMs (Graf and Dillmann, 1999). As shown in Fig. 2, MPMs can be

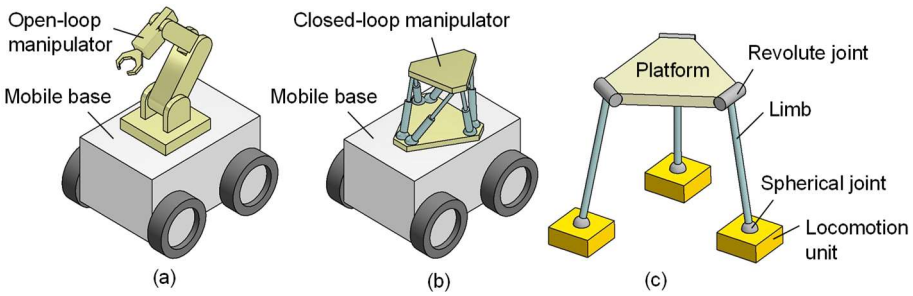

Fig. 1 Mobile robots with (a) serial and (b) parallel manipulators, and (c) three-limb mobile parallel manipulator.

Paper No.22-00271
[DOI: 10.1299/jamdsm.2023jamdsm0020]

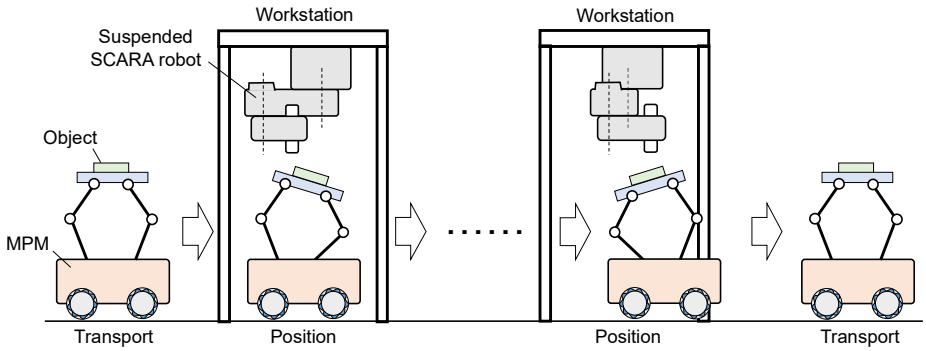

Fig. 2 Industrial application of mobile parallel manipulators (MPMs).

applied in automated production lines to transport and position objects. The layout of MPMs can be flexibly designed for a given factory environment. If an MPM fails, it can be immediately replaced by another one, which increases the capacity utilization rate.

Conventional MPMs have more than six actuators to independently actuate the 3-DOF planar motions of the mobile base and the 6-DOF spatial motions of the manipulator, leading to kinematic redundancy. This raises the cost of the development and deployment of the production lines shown in Fig. 2. To solve this problem, an MPM composed of a platform and three limbs [see Fig. 1(c)] has been proposed (Tsai and Tahmasebi, 1993; Ben-Horin, et al., 1998; Shoval and Shoham, 2001; Ben-Horin, et al., 2006). One end of each limb is connected to a 2-DOF locomotion unit, and the other end is connected to the platform. Our previous research discussed the type synthesis of three-limb MPMs (Long, et al., 2022) and proposed a slidable-wheeled mobile base for them (Terakawa, et al., 2018, 2019).

However, such 6-DOF MPMs still have at least six motors. To further reduce the number of motors, this paper proposes a nonholonomic MPM, named VErsatile MObile PArallel Manipulator (VEMOPAM), which is actuated by two two-wheel-drive (2WD) carts. The motions of the carts are transmitted to a platform via a single-loop parallel mechanism that consists of three screw pairs. The 6-DOF pose of the platform is set using only four motors, which are mounted on the carts. Compared with the conventional MPMs, VEMOPAM has fewer motors, which leads to weight and cost reductions. In addition, whereas a three-limb MPM has multiple loops in its parallel structure, VEMOPAM has only one loop and thus occupies a smaller area. Therefore, VEMOPAM is considered to be more applicable for the production lines shown in Fig. 2.

To move the platform of VEMOPAM to the desired pose, an appropriate path planning method for the two carts is necessary. Path planners for mobile robots based on a variety of algorithms, such as genetic algorithms (Shibata, et al., 1992, 1993) and recursive subdivision algorithms (Laumond, et al., 1994), have been proposed (Tsubouchi, et al., 1994; Stentz, 1994; Stentz and Hebert, 1995; Moon, et al., 1999; Koenig and Likhachev, 2002; Seki, et al., 2005; AL-Taharwa, et al., 2008; Lamini, et al., 2018). Path planning and control approaches for multi-mobile-robot systems have also been proposed (Hashimoto, et al., 1995; Kosuge, et al., 1997, 1998, 1999). However, due to the complicated constraint conditions (e.g., nonholonomic constraints and stroke of the screw pairs) and the unique structural characteristics (e.g., singularities) of VEMOPAM, none of the above path planning methods can be used to optimize the paths of the two carts. In this paper, a custom path planning method that has four steps is presented for VEMOPAM. This method does not provide optimal paths for the carts. Nevertheless, it can be easily realized with low computational cost because the paths can be planned without considering the complex constraint conditions of VEMOPAM. We analyze the movements of VEMOPAM in each step using simulations. Moreover, an experimental prototype of VEMOPAM is constructed to demonstrate the usefulness of the proposed mechanism and path planning method.

Symbols given in Table 1 are used to clearly illustrate the structure and features of the proposed mechanism.

2. Proposed novel mobile parallel manipulator

This section shows the structure and motions of VEMOPAM.

[DOI: 10.1299/jamdsm.2023jamdsm0020]

Table 1 Main symbols used for analysis.

Symbol	Specification	Symbol	Specification
$\boldsymbol{G}$	Nonholonomic constraint matrix.	$\boldsymbol{q}_{\mathrm{ini}}, \boldsymbol{q}_{\mathrm{tar}}$	Initial and target pose vectors of platform.
i	Subscript used to distinguish two carts.	r	Radius of drive wheels of carts.
$\boldsymbol{J}$	Jacobian matrix of inverse kinematics.	r_c	Radius of sector path in second step of FSPP method.
K_x, K_y, K_z	Constants in Kanayama's control rule.	v_0	Rated translational velocity of carts.
l_1, l_2, l_3, l_s	Lengths of linkages of VEMOPAM.	v_1, v_2	Translational velocities of carts.
$l_{\mathrm{scon}}, z_{\mathrm{con}}$	Constants.	w	Distance between CP and wheels of cart.
$N_{\mathrm{dof}}, N_{\mathrm{link}}, N_{\mathrm{joint}}$	Numbers of DOFs, links, and joints.	$\{x, y, z\}$	Position of platform.
O–XYZ	Fixed reference frame.	$\{x_{a,i}, y_{a,i}, \phi_{a,i}\}$	Actual positions and angles of rotation of carts.
$O_{c,i}$–$X_{c,i}Y_{c,i}Z_{c,i}$	Cart reference frame.	$\{x_{e,i}, y_{e,i}, \phi_{e,i}\}$	Differences between planned and actual positions and angles of rotation of carts.
O_p–$X_pY_pZ_p$	Platform reference frame.	$\{x_i, y_i, \phi_i\}$	Planned positions and angles of rotation of carts.
$\boldsymbol{p}$	Pose vector of carts.	$\Delta\phi_1, \cdots, \Delta\phi_8$	Rotational angles of carts in four steps of FSPP method.
p_1	Lead of screw pairs B1-C1 and B2-C2.	$\{\phi_x, \phi_y, \phi_z\}$	Orientation angles (yaw, pitch, and roll) of platform.
p_2	Lead of screw pair B3-C3.	ω_0	Rated rotational velocities of carts.
$\boldsymbol{p}_{\mathrm{ini}}, \boldsymbol{p}_{\mathrm{tar}}$	Initial and target pose vectors of carts.	ω_1, ω_2	Rotational velocities of carts.
$\boldsymbol{q}$	Pose vector of platform.	$\omega_{l,i}, \omega_{r,i}$	Speeds of two drive wheels of carts.

2.1 Structure of proposed mobile parallel manipulator

Figure 3 shows the structure of VEMOPAM. VEMOPAM has two 2WD carts (A1 and A2), each of which has two drive wheels installed on the left and right sides, respectively, and two auxiliary wheels installed on the front and back sides, respectively, to maintain balance. The projected point of the midpoint between the two drive wheels on the floor is defined as the center point (CP) of the cart. Two screw shafts (B1 and B2) are respectively fixed on A1 and A2 so that they can move together. The center axes of B1 and B2 pass through the CPs of A1 and A2, respectively. Screw

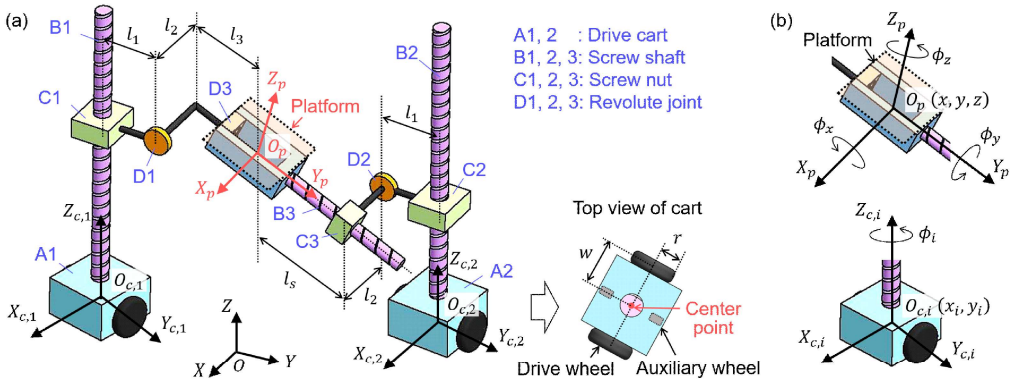

Fig. 3 Proposed VEMOPAM: (a) structure and reference frames; (b) definitions of poses.

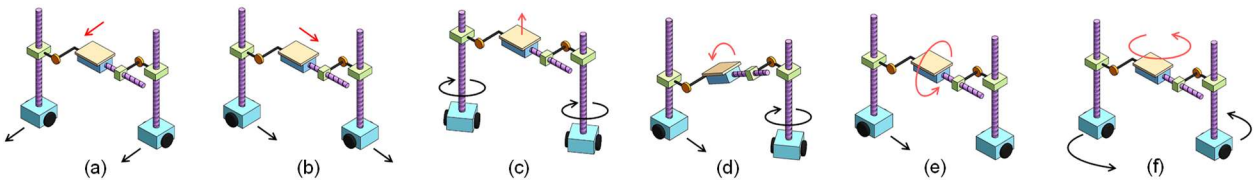

Fig. 4 Basic movements of VEMOPAM: (a–c) 3-DOF translational movements and (d–f) 3-DOF rotational movements of platform.

[DOI: 10.1299/jamdsm.2023jamdsm0020]

shafts B1, B2, and B3, and screw nuts C1, C2, and C3 form three screw pairs; revolute joints D1 and D2 form two revolute pairs of the linkages; and revolute joint D3 forms a revolute pair of the linkages and the platform. Therefore, the motions of A1 and A2 are transmitted to the platform via a parallel mechanism composed of three screw pairs (B1-C1, B2-C2, and B3-C3) and three revolute pairs (D1, D2, and D3).

The number of geometric DOFs of VEMOPAM N_{dof} is calculated by Gruebler's equation as follows:

$$N_{\mathrm{dof}} = 6\left(N_{\mathrm{link}} - N_{\mathrm{joint}} - 1\right) + \sum_{j=1}^{N_{\mathrm{joint}}} f_i, \tag{1}$$

where N_{link} is the total number of links, N_{joint} is the total number of joints, and f_j indicates the number of DOFs of each joint. The mechanism of VEMOPAM has eight links; each of the joints between carts A1 and A2 and the floor has three geometric DOFs, and each of the other joints has one DOF. Therefore, $N_{\mathrm{link}} = 8$, $N_{\mathrm{joint}} = 8$, and $\sum f_i = 2 \times 3 + 6 \times 1 = 12$. From Eq. (1), it can be confirmed that VEMOPAM has six geometric DOFs ($N_{\mathrm{dof}} = 6$).

2.2 Definitions of reference frames and pose

To describe the pose of VEMOPAM, some reference frames are defined as shown in Fig. 3(a). $O{-}XYZ$ is defined as a fixed frame, and $O{-}XY$ is the floor on which the carts move. Platform frame $O_p{-}X_pY_pZ_p$ is fixed at the platform. Axis Y_p coincides with the center axis of screw shaft B3. Two cart frames $O_{c,i}{-}X_{c,i}Y_{c,i}Z_{c,i}$ are fixed to carts A1 and A2. Origins $O_{c,i}$ are the CPs and correspond to the center of rotation of the carts. Axes $X_{c,i}$ and $Y_{c,i}$ are respectively the forward and left lateral directions of the carts. Axes $Z_{c,1}$ and $Z_{c,2}$ coincide with the center axes of screw shafts B1 and B2, respectively. In this paper, we use the subscript $i = 1, 2$ to represent A1 and A2, respectively.

As shown in Fig. 3(b), with respect to $O{-}XYZ$, the position of the platform is defined by the position $\{x, y, z\}$ of O_p. The orientation of the platform is represented using three angles of rotation around axes X_p, Y_p, and Z_p, i.e., yaw ϕ_x, pitch ϕ_y, and roll ϕ_z, respectively. We define the reference orientation of the platform to be $\phi_x = \phi_y = \phi_z = 0$ (i.e., the directions of X_p, Y_p, and Z_p are respectively the same as those of X, Y, and Z). After the platform is rotated about the three axes in the order of Z_p, X_p, and Y_p, it changes from the reference orientation to the current orientation, and ϕ_x, ϕ_y, and ϕ_z become the current values.

2.3 Movements of carts and platform

As shown in Fig. 4, the pose $\{x, y, z, \phi_x, \phi_y, \phi_z\}$ of the platform can be controlled by moving A1 and A2. Fig. 4(a)–(c) show that $\{x, y, z\}$ is changed if A1 and A2 translate or rotate with the same direction and velocity; Fig. 4(d) shows that ϕ_x is changed if nuts C1 and C2 move vertically with different velocities; Fig. 4(e) shows that ϕ_y is changed due to the screw motions of screw pair B3-C3; Fig. 4(f) shows that ϕ_z is changed if A1 and A2 revolve in concentric circles.

The movement shown in Fig. 4(e), i.e., the change of ϕ_y, is considered to be extremely difficult if B3-C3 has a small lead. For example, if the lead of B3-C3 is 20 mm/r, even a small error of 1 mm in the linear motion of nut C3 in Y_p would cause an 18° deviation of ϕ_y. This is a drawback of this mechanism. This study addresses this problem by using a speed reducer when realizing a prototype of VEMOPAM. The details are described in Section 6.1.

3. Kinematics of VEMOPAM

Prior to the discussion of the path planning method, we analyze the kinematics of VEMOPAM in this section to clarify its motion conditions.

3.1 Inverse kinematics

For parallel mechanisms, inverse kinematics is easier than forward kinematics (Arai, 1992). Here, VEMOPAM is treated as a movable parallel mechanism and its inverse kinematics is considered. Under the assumptions that: i) the floor is flat and smooth; ii) rigid shafts B1 and B2 remain vertical and do not vibrate during low-velocity movements,

[DOI: 10.1299/jamdsm.2023jamdsm0020]

the following equations are established to represent the geometric relations among the parts of VEMOPAM.

$$\begin{aligned}
x_1 &= x + l_1 \sin\phi_z + l_2 \cos\phi_z + l_3 \cos\phi_x \sin\phi_z, \\
y_1 &= y - l_1 \cos\phi_z + l_2 \sin\phi_z - l_3 \cos\phi_x \cos\phi_z, \\
\phi_1 &= \phi_z - \frac{2\pi}{p_1}(z - z_{\mathrm{con}} - l_3 \sin\phi_x), \\
x_2 &= x - l_1 \sin\phi_z - l_2 \cos\phi_z - l_s \cos\phi_x \sin\phi_z, \\
y_2 &= y + l_1 \cos\phi_z - l_2 \sin\phi_z + l_s \cos\phi_x \cos\phi_z, \\
\phi_2 &= \phi_z - \frac{2\pi}{p_1}(z - z_{\mathrm{con}} + l_s \sin\phi_x),
\end{aligned} \tag{2}$$

where $\{x_i, y_i, \phi_i\}$ represents the poses, i.e., the positions $\{x_i, y_i\}$ and the angles of rotation ϕ_i, of carts A1 and A2 with respect to O–XYZ $(i = 1, 2)$, l_1, l_2, l_3, and l_s are the lengths of the linkages (see Fig. 3), p_1 is the lead of screw pairs B1-C1 and B2-C2, and z_{con} is a constant. The value of l_s varies depending on the screw motions of screw pair B3-C3:

$$l_s = l_{\mathrm{scon}} - \frac{p_2 \phi_y}{2\pi}, \tag{3}$$

where p_2 is the lead of B3-C3 and l_{scon} is a constant.

By rearranging Eq. (2), several equations that describe the special geometric features of VEMOPAM can be obtained. Equation (4) can be derived by rearranging the first, second, fourth, and fifth equations of Eq. (2).

$$(x_1 - x_2)\cos\phi_z + (y_1 - y_2)\sin\phi_z = 2l_2. \tag{4}$$

Equation (4) shows that the roll ϕ_z of the platform depends on only the relative position of the carts. The condition $x_1 - x_2 = y_1 - y_2 = 0$ (i.e., A1 and A2 collide with each other) is never satisfied as long as $l_2 > 0$. In addition, Eq. (5) can be derived by rearranging the third and sixth equations of Eq. (2).

$$\phi_1 - \phi_2 = \frac{2\pi}{p_1}(l_3 + l_s)\sin\phi_x. \tag{5}$$

Equation (5) shows the relation between the difference in the angles of rotation of the carts $(\phi_1 - \phi_2)$ and the yaw ϕ_x and pitch ϕ_y of the platform.

Differentiating Eq. (2) with respect to time yields Eq. (6).

$$\dot{\boldsymbol{p}} = \boldsymbol{J}\dot{\boldsymbol{q}}. \tag{6}$$

Here, $\boldsymbol{p}$, $\boldsymbol{q}$, and the Jacobian matrix $\boldsymbol{J}$ are given in Eq. (7).

$$\begin{aligned}
&\boldsymbol{p} = \{x_1, y_1, \phi_1, x_2, y_2, \phi_2\}^T, \boldsymbol{q} = \{x, y, z, \phi_x, \phi_y, \phi_z\}^T, \\
&\boldsymbol{J} = \begin{bmatrix}
1 & 0 & 0 & -l_3 \sin\phi_x \sin\phi_z & 0 & (l_1 + l_3\cos\phi_x)\cos\phi_z - l_2\sin\phi_z \\
0 & 1 & 0 & l_3 \sin\phi_x \cos\phi_z & 0 & (l_1 + l_3\cos\phi_x)\sin\phi_z + l_2\cos\phi_z \\
0 & 0 & -2\pi/p_1 & 2\pi l_3 \cos\phi_x / p_1 & 0 & 1 \\
1 & 0 & 0 & l_s \sin\phi_x \sin\phi_z & p_2 \cos\phi_x \sin\phi_z/(2\pi) & -(l_1 + l_s\cos\phi_x)\cos\phi_z + l_2\sin\phi_z \\
0 & 1 & 0 & -l_s \sin\phi_x \cos\phi_z & -p_2 \cos\phi_x \cos\phi_z/(2\pi) & -(l_1 + l_s\cos\phi_x)\sin\phi_z - l_2\cos\phi_z \\
0 & 0 & -2\pi/p_1 & -2\pi l_s \cos\phi_x / p_1 & p_2 \sin\phi_x / p_1 & 1
\end{bmatrix}.
\end{aligned} \tag{7}$$

We consider the rolling-without-slipping condition for the carts and express the nonholonomic constraints using Eq. (8).

$$\boldsymbol{G}\dot{\boldsymbol{p}} = \boldsymbol{0}. \tag{8}$$

Here, $\boldsymbol{G}$ is given in Eq. (9).

[DOI: 10.1299/jamdsm.2023jamdsm0020]

$$\boldsymbol{G} = \begin{bmatrix} -\sin\phi_1 & \cos\phi_1 & 0 & 0 & 0 & 0 \\ 0 & 0 & 0 & -\sin\phi_2 & \cos\phi_2 & 0 \end{bmatrix}. \tag{9}$$

Substituting Eq. (6) into Eq. (8) yields the following equation,

$$\boldsymbol{G}\boldsymbol{J}\dot{\boldsymbol{q}} = \boldsymbol{0}. \tag{10}$$

Equation (10) shows the effect of the nonholonomic constraints on the movements of VEMOPAM.

3.2 Singular and failure configuration

Parallel mechanisms have two kinds of singularity (Gosselin and Angeles, 1990). The first kind occurs when $\det\left(\boldsymbol{J}^{-1}\right) = 0$, and the second kind occurs when $\det(\boldsymbol{J}) = 0$. An analysis based on the obtained $\boldsymbol{J}$ indicates that the second kind occurs when Eq. (11) is satisfied.

$$\cos\phi_x = -\frac{2l_1}{l_3 + l_s}. \tag{11}$$

Figure 5(a) shows that VEMOPAM falls into the second kind of singular configuration if the line of the CPs of the carts is normal to the projection of the center axis of screw shaft B3 on the floor. As shown in Fig. 5(b), with this singular configuration, if carts A1 and A2 are commended to move far away from each other, because the direction of the screw motion of B3-C3 is no longer constrained, the platform has two possible poses (A and B) after moving. Because the right-hand side of Eq. (11) is negative, this singularity does not occur if $-\pi/2 \le \phi_x \le \pi/2$.

The above analysis was performed based on the premise that the axes of rotation of revolute joints D1 and D2 are always parallel due to the structural constraints of VEMOPAM. However, as shown in Fig. 6, when the center axis of screw shaft B3 becomes perpendicular to the floor (i.e., $\phi_x = \pm\pi/2$), the constraint condition for VEMOPAM changes. At this instant, if the carts revolve about the center axis of B3, the parallelism of D1 and D2 cannot be maintained, and the geometric relations represented by Eq. (2) no longer hold. In this paper, this configuration is referred to as the failure configuration.

From the above analysis, it was confirmed that if ϕ_x is limited to be $-\pi/2 < \phi_x < \pi/2$, VEMOPAM can avoid the singular and failure configurations, and that the pose of the platform has a one-to-one correspondence with the poses of carts A1 and A2. On the other hand, since the workspace of the platform is limited due to the strokes of the screw pairs, the first kind of singular configuration may occur if the platform reaches the boundary of its workspace. Based on these analysis results, a path planning method is proposed for the two carts in the next section.

4. Path planning for carts

In this section, a path planning method for carts A1 and A2 of VEMOPAM is presented. We use the vectors $\boldsymbol{q}_{\text{ini}}$ and $\boldsymbol{q}_{\text{tar}}$ to respectively represent the initial and target poses of the platform.

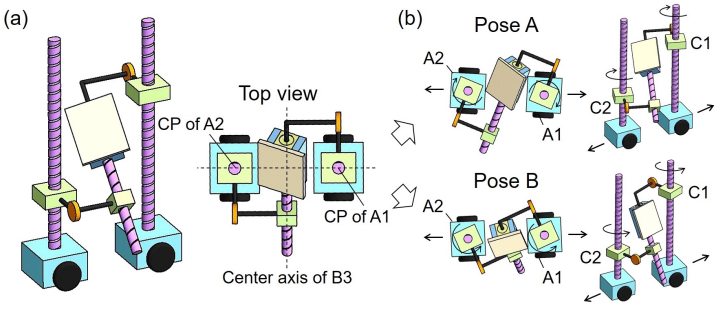

Fig. 5 Singularity analysis results for VEMOPAM: (a) singular configuration and (b) motions in this configuration.

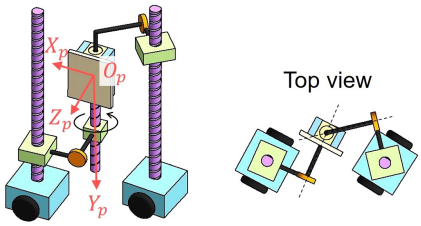

Fig. 6 Failure configuration for VEMOPAM.

[DOI: 10.1299/jamdsm.2023jamdsm0020]

$$\begin{aligned} \boldsymbol{q}_{\text{ini}} &= \{x_0, y_0, z_0, \phi_{x0}, \phi_{y0}, \phi_{z0}\}^T, \\ \boldsymbol{q}_{\text{tar}} &= \{x_t, y_t, z_t, \phi_{xt}, \phi_{yt}, \phi_{zt}\}^T. \end{aligned} \tag{12}$$

Substituting Eq. (12) into Eq. (2) yields the vectors $\boldsymbol{p}_{\text{ini}}$ and $\boldsymbol{p}_{\text{tar}}$, which respectively represent the initial and target poses of A1 and A2.

$$\begin{aligned} \boldsymbol{p}_{\text{ini}} &= \{x_{10}, y_{10}, \phi_{10}, x_{20}, y_{20}, \phi_{20}\}^T, \\ \boldsymbol{p}_{\text{tar}} &= \{x_{1t}, y_{1t}, \phi_{1t}, x_{2t}, y_{2t}, \phi_{2t}\}^T. \end{aligned} \tag{13}$$

When A1 and A2 reach their target poses, the platform also reaches its target pose. However, with the nonholonomic constraints, the six outputs of VEMOPAM, i.e., the 6-DOF pose of the platform $\{x, y, z, \phi_x, \phi_y, \phi_z\}$, cannot be simultaneously controlled by the four inputs, i.e., the speeds of the drive wheels of the carts. Our solution is to divide the path planning process into several steps. In each of the steps, fewer than four outputs are changed; the other outputs are fixed by the structural constraints. After the final step, all six outputs will have reached their target values. The following constraint conditions for VEMOPAM are considered in the design of the algorithm:

1) Due to the nonholonomic constraints, the motions of A1 and A2 in their lateral directions are restricted. As indicated in Eq. (10), these nonholonomic constraints for A1 and A2 may interact with each other via the parallel mechanism. Thus, the carts cannot move in a particular direction without some maneuvers, such as a turnabout.
2) For the miniaturization of VEMOPAM, screw pair B3-C3 should have a short stroke. This may increase the risk that nut C3 moves too far and hits at the end of the stroke of screw shaft B3. Therefore, the motions of the carts must be limited to ensure the safe use of B3-C3.
3) As described in Section 2.3, the pitch ϕ_y of the platform may be sensitive to the screw motions of B3-C3. To stabilize the motions of the platform, ϕ_y should not be changed for most of the movement time.

Such unique and complicated constraint conditions are not considered in conventional path planning methods. A custom path planning method that consists of four steps, named the Four-Step Path Planning (FSPP) method, is thus proposed for VEMOPAM. The first step is planned to move cart A1 to its target position, the second and third steps are planned to move cart A2 to its target position, and the fourth step is planned to rotate A1 and A2 until they reach the target angles of rotation. A detailed description of each step is given below.

4.1 First step

Figure 7 shows the motions of A1 and A2 and the variation of the pose of the platform in the first step. A1 and A2 are expected to reach their target positions with a long-distance translation. If A1 and A2 directly move to their target positions, because of the screw movement of B3-C3, the pitch ϕ_y of the platform may greatly change, and C3 may hit at the end of the stroke, which is inconsistent with the path planning goals. To stabilize the motions of the platform, in the first step, a path is planned only for A1 to reach its target position; another path that is parallel to the path of A1 is planned for A2. In this step, two outputs, namely x and y, of the platform are changed.

A preliminary operation for this step, i.e., rotating A1 and A2, is necessary due to the nonholonomic constraints. The initial angles of rotation of A1 and A2, i.e., ϕ_{10} and ϕ_{20}, are represented in the following form:

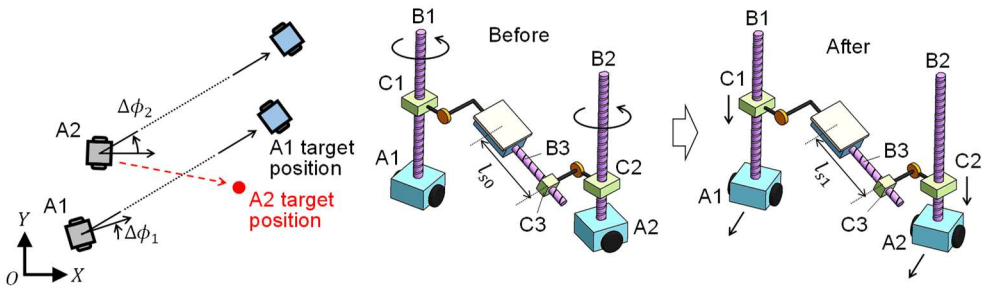

Fig. 7 Paths of carts and motions of platform in first step of path planning.

[DOI: 10.1299/jamdsm.2023jamdsm0020]

$$\begin{aligned}\phi_{10} &= 2n_1\pi + \hat{\phi}_{10} \ \ (n_1 \in \mathbf{N}, -\pi < \hat{\phi}_{10} < \pi),\\ \phi_{20} &= 2n_2\pi + \hat{\phi}_{20} \ \ (n_2 \in \mathbf{N}, -\pi < \hat{\phi}_{20} < \pi).\end{aligned} \tag{14}$$

Then, A1 is rotated at an angle of $\Delta\phi_1$ to set its forward or backward direction toward its target position. Simultaneously, A2 is rotated at an angle of $\Delta\phi_2$ so that its forward direction is parallel to the forward direction of A1. We use ϕ_{10} and ϕ_{20} given in Eq. (14) to represent $\Delta\phi_1$ and $\Delta\phi_2$ as follows:

$$\begin{aligned}\Delta\phi_i &= \begin{cases}\Delta\phi_i' & (\text{if} \ \ -\pi/2 \le \Delta\phi_i' < \pi/2),\\ \Delta\phi_i' - \pi & (\text{if} \ \ \Delta\phi_i' \ge \pi/2),\\ \Delta\phi_i' + \pi & (\text{if} \ \ \Delta\phi_i' < -\pi/2),\end{cases} \qquad (i = 1, 2),\\ \Delta\phi_1' &= \tan^{-1}\frac{y_{1t} - y_{10}}{x_{1t} - x_{10}} - \hat{\phi}_{10}, \Delta\phi_2' = \tan^{-1}\frac{y_{1t} - y_{10}}{x_{1t} - x_{10}} - \hat{\phi}_{20}.\end{aligned} \tag{15}$$

Equations (14) and (15) guarantee that $|\Delta\phi_i| \le \pi/2 \ \ (i = 1, 2)$, which minimizes movement time. The rotational velocities of A1 and A2, which are respectively represented as ω_1 and ω_2, are set to $\omega_1 = \omega_2 = \omega_0$, where ω_0 is a rated rotational velocity. The angles of rotation for the carts after rotation are expressed in the following form:

$$\begin{aligned}\phi_{10} + \Delta\phi_1 &= 2n_1'\pi + \hat{\phi}_1,\\ \phi_{20} + \Delta\phi_2 &= 2n_2'\pi + \hat{\phi}_1, (n_1', n_2' \in \mathbf{N}, -\pi < \hat{\phi}_1 < \pi).\end{aligned} \tag{16}$$

After the rotations of A1 and A2, if $\Delta\phi_1 \ne \Delta\phi_2$, the length of l_s may change from the initial value l_{s0} to l_{s1} due to the screw movement of B3-C3. l_{s1} is expressed as follows:

$$\begin{aligned}l_{s1} &= -l_3 + \sqrt{a^2 + b^2},\\ a &= -2l_1 + (x_{10} - x_{20})\sin\phi_{z0} - (y_{10} - y_{20})\cos\phi_{z0},\\ b &= \frac{p_1}{2\pi}(\phi_{10} + \Delta\phi_1 - \phi_{20} - \Delta\phi_2).\end{aligned} \tag{17}$$

Because the difference between $\Delta\phi_1$ and $\Delta\phi_2$ is small, the change of l_s, i.e., $|l_{s1} - l_{s0}|$, is very small. By selecting a proper stroke for B3-C3, l_{s1} can be limited within the stroke of B3-C3.

Next, A1 and A2 move at the same velocity until A1 reaches its target position. Their translational velocities, which are respectively represented as v_1 and v_2, are set to $v_1 = v_2 = v_0$, where v_0 is a rated translational velocity.

4.2 Second step

Figure 8 shows the motions of A1 and A2 and the variation of the pose of the platform in the second step. After A1 is moved to its target position in the previous step, if A2 is also moved to its target position along the shortest path (red path in Fig. 8), due to the screw movement of B3-C3, ϕ_y would be greatly changed, and C3 may hit at the end of the stroke. To keep ϕ_y unchanged, A1 needs to be rotated to move nut C1 vertically. However, such a movement can greatly change the other five outputs, i.e., x, y, z, ϕ_x, and ϕ_z. Therefore, we designed the second and third steps so as to indirectly move A2 to its target position. The second step mainly changes three outputs, namely x, y, and ϕ_z, and sets ϕ_z to the target value ϕ_{zt}.

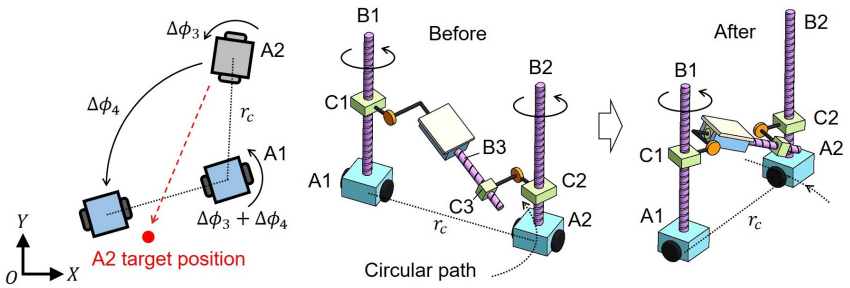

Fig. 8 Paths of carts and motions of platform in second step of path planning.

[DOI: 10.1299/jamdsm.2023jamdsm0020]

A preliminary operation, i.e., rotating A1 and A2 at the same angle of $\Delta\phi_3$, is necessary. To minimize the movement time, $\Delta\phi_3$ is calculated as follows:

$$\Delta\phi_3 = \begin{cases} \Delta\phi_3' & \left(\text{if } -\pi/2 \le \Delta\phi_3' < \pi/2\right), \\ \Delta\phi_3' - \pi & \left(\text{if } \Delta\phi_3' \ge \pi/2\right), \\ \Delta\phi_3' + \pi & \left(\text{if } \Delta\phi_3' < -\pi/2\right), \end{cases} \tag{18}$$
$$\Delta\phi_3' = \tan^{-1}\frac{y_{10} - y_{20}}{x_{10} - x_{20}} - \hat{\phi}_1 + \pi/2.$$

As done in the previous step, the rotational velocities of A1 and A2 are set to $\omega_1 = \omega_2 = \omega_0$. After rotation, the forward directions of A1 and A2 are both normal to the line of their CPs.

Then, a sector path for A2 is generated. The center of this path is the CP of A1, the radius r_c is the distance between the CPs of A1 and A2. We can calculate r_c using the initial positions of A1 and A2 as follows:

$$r_c = \sqrt{(x_{10} - x_{20})^2 + (y_{10} - y_{20})^2}. \tag{19}$$

The central angle $\Delta\phi_4$ of the sector path is set to

$$\Delta\phi_4 = \phi_{zt} - \phi_{z0}. \tag{20}$$

A2 moves on this path with a uniform velocity. Simultaneously, A1 rotates about its own CP in the same direction as that of the revolution of A2 to maintain the three outputs, i.e., z, ϕ_x, and ϕ_y, unchanged. The translational and rotational velocities of A1 and A2 are given as follows:

$$v_1 = 0, v_2 = v_0, \omega_1 = \omega_2 = v_0/r_c. \tag{21}$$

The angles of rotation for the carts after this step are expressed in the following form:

$$\begin{aligned} &\phi_{10} + \Delta\phi_1 + \Delta\phi_3 + \Delta\phi_4 = 2n_1''\pi + \hat{\phi}_2, \\ &\phi_{20} + \Delta\phi_2 + \Delta\phi_3 + \Delta\phi_4 = 2n_2''\pi + \hat{\phi}_2, \left(n_1'', n_2'' \in \mathbf{N}, -\pi < \hat{\phi}_2 < \pi\right). \end{aligned} \tag{22}$$

As indicated in Eq. (4), ϕ_z depends on only the relative positions of the carts. After the revolution of A2, ϕ_z changes from the initial value ϕ_{z0} to the target value ϕ_{zt}. In the next two steps, ϕ_z is kept unchanged.

4.3 Third step

Figure 9 shows the motions of A1 and A2 and the variation of the pose of the platform in the third step. This step is planned so as to move A2 to its target position. In this step, fewer than four outputs other than ϕ_z are simultaneously changed.

A1 and A2 are rotated at the same angle of $\Delta\phi_5$ before this step. The following equation, whose form is similar to Eq. (15), is used to calculate $\Delta\phi_5$:

$$\Delta\phi_5 = \begin{cases} \Delta\phi_5' & \left(\text{if } -\pi/2 \le \Delta\phi_5' < \pi/2\right), \\ \Delta\phi_5' - \pi & \left(\text{if } \Delta\phi_5' \ge \pi/2\right), \\ \Delta\phi_5' + \pi & \left(\text{if } \Delta\phi_5' < -\pi/2\right), \end{cases} \tag{23}$$
$$\Delta\phi_5' = \tan^{-1}\frac{y_{2t} - {}^3y_{20}}{x_{2t} - {}^3x_{20}} - \hat{\phi}_2,$$

[DOI: 10.1299/jamdsm.2023jamdsm0020]

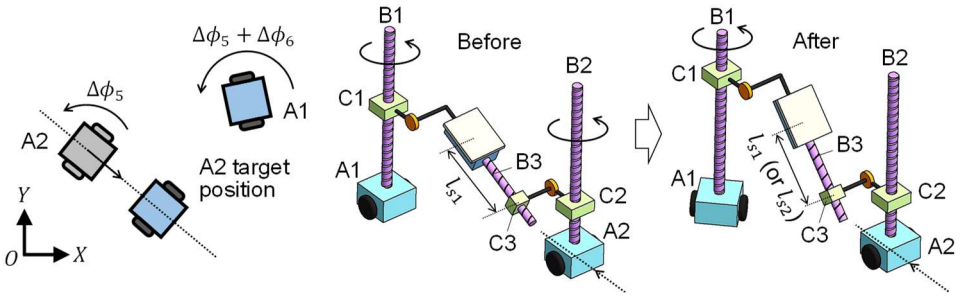

Fig. 9 Paths of carts and motions of platform in third step of path planning.

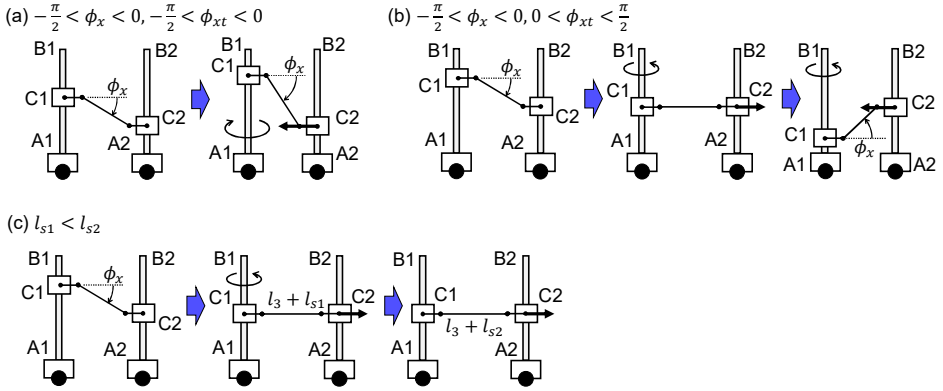

Fig. 10 Examples of movements of nuts C1 and C2 in third step of path planning for (a) Case I, $-\pi/2 < \phi_x < 0$ and $-\pi/2 < \phi_{xt} < 0$; (b) Case II, $-\pi/2 < \phi_x < 0$ and $0 < \phi_{xt} < \pi/2$; and (c) Case III, $l_{s1} < l_{s2}$.

where $({}^3x_{20}, {}^3y_{20})$ indicates the position of A2 at the start of the third step and can be obtained from the previous two steps. As done in the previous steps, the rotational velocities of A1 and A2 are set to $\omega_1 = \omega_2 = \omega_0$. After rotation, the forward or backward direction of A2 is set toward its target position.

Then, a linear path for A2 is planned. By substituting the target position (x_{1t}, y_{1t}) of A1 and target roll ϕ_{zt} of the platform into Eq. (4), the following equation can be obtained,

$$(x_{1t} - x_2)\cos\phi_{zt} + (y_{1t} - y_2)\sin\phi_{zt} = 2l_2. \tag{24}$$

This equation is represented by the dotted lines shown in Fig. 9. If A1 is fixed at the target position and A2 is moved along this line, ϕ_z can be kept at the target value ϕ_{zt} due to the structural constraints of VEMOPAM. The movement direction of A2 is decided so as to limit the motions of B3-C3 within its stroke. We use the following three cases, shown in Fig. 10, to explain how to decide the motions of the carts.

1) Case I

As shown in Fig. 10(a), at the start of the third step, if the yaw ϕ_x of the platform and its target value ϕ_{xt} satisfy the condition $\phi_x\phi_{xt} \geq 0$, A2 directly moves to its target position. At the same time, A1 is rotated to move nut C1 up or down to maintain length l_s at l_{s1}.

2) Case II

As shown in Fig. 10(b), at the start of the third step, if ϕ_x and ϕ_{xt} satisfy the condition $\phi_x\phi_{xt} < 0$, A2 initially moves away from its target position until $\phi_x = 0$. A2 then moves in the opposite direction to approach its target position. At the same time, A1 is rotated to maintain length l_s at l_{s1}.

During the motions in Cases I and II, the two outputs ϕ_y and ϕ_z do not change. These motions are planned so as to make ϕ_x and ϕ_{xt} satisfy $\phi_x\phi_{xt} \geq 0$. The reason for this is explained in Section 4.4.

3) Case III

As shown in Fig. 10(c), when A2 reaches its target position, length l_s may increase. In this case, A2 initially moves toward its target position and A1 rotates to maintain l_s at l_{s1}. Similarly, ϕ_y and ϕ_z are not changed during the motion. When C1 reaches the height of C2 (i.e., the angles of rotation of the carts are the same, $\phi_1 = \phi_2$), A1 stops rotating but A2 continues moving, which changes l_s from l_{s1} to l_{s2} ($l_{s1} < l_{s2}$). The change in l_s can be limited within the stroke of B3-C3, which is explained in Section 4.4. Only ϕ_y is changed during this motion.

[DOI: 10.1299/jamdsm.2023jamdsm0020]

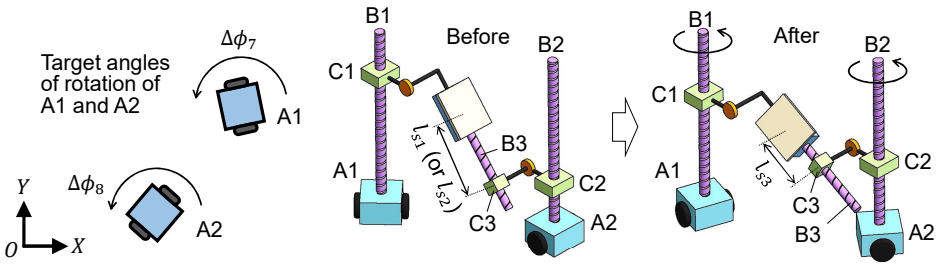

Fig. 11 Paths of carts and motions of platform in fourth step of path planning.

We now describe the displacements and velocities of A1 and A2 in the above three cases in detail. By rearranging the first, second, fourth, and fifth equations of Eq. (2), the following equation can be obtained.

$$\cos\phi_x = \frac{(x_1 - x_2)\sin\phi_z - (y_1 - y_2)\cos\phi_z - 2l_1}{l_3 + l_s}. \tag{25}$$

After substituting the target positions of the carts, i.e., (x_{1t}, y_{1t}) and (x_{2t}, y_{2t}), the target roll $\phi_z = \phi_{zt}$, and $l_s = l_{s1}$ into Eq. (25), if the absolute value of the right-hand side of Eq. (25) is smaller than 1, i.e., $|(x_{1t} - x_{2t})\sin\phi_{zt} - (y_{1t} - y_{2t})\cos\phi_{zt} - 2l_1| \le l_3 + l_{s1}$, the methods described in Cases I and II are used to plan paths. In these cases, the rotational velocity of A1 is set to $\omega_1 = 4\omega_0$, based on which ϕ_1 at each moment can be easily obtained. During the linear motion of A2, ϕ_2 does not change. Therefore, we can substitute the values of ϕ_1 and ϕ_2 and $l_s = l_{s1}$ into Eq. (5) to calculate the time-varying value ϕ_x. Then, substituting the obtained ϕ_x, the target position (x_{1t}, y_{1t}) of A1, the target roll ϕ_{zt}, and $l_s = l_{s1}$ into Eq. (25) yields the following equation.

$$\cos\phi_x = \frac{(x_{1t} - x_2)\sin\phi_{zt} - (y_{1t} - y_2)\cos\phi_{zt} - 2l_1}{l_3 + l_{s1}}. \tag{26}$$

By using Eqs. (24) and (26), the position (x_2, y_2) of A2 at each moment can be planned.

The method described in Case III is used to plan paths if $|(x_{1t} - x_{2t})\sin\phi_{zt} - (y_{1t} - y_{2t})\cos\phi_{zt} - 2l_1| > l_3 + l_{s1}$. The position of A2 can be calculated using the same method used in Cases I and II until A1 stops rotating. When $\phi_1 = \phi_2$, A1 stops rotating and A2 continues moving with the velocity $v_2 = v_0$.

4.4 Fourth step

Figure 11 shows the motions of A1 and A2 and the variation of the pose of the platform in the fourth step. This step is planned so as to rotate A1 and A2 multiple times until they reach the target angles of rotation (ϕ_{1t} and ϕ_{2t}). After this final step, all six outputs will have reached their target values.

Here, an explanation for Cases I, II, and III of the third step (see above) is given. For example, if the value of ϕ_x before the fourth step is $-\pi/4$ and its target value ϕ_{xt} is $\pi/4$, during the fourth step, ϕ_x first changes from $-\pi/4$ to 0 and then changes to $\pi/4$. When ϕ_x becomes 0, nuts C1 and C2 reach the same height and length l_s becomes its shortest value. At this time, nut C3 may hit at the end of its stroke. To avoid this problem, we use the methods described in Cases I and II to ensure that $\phi_x\phi_{xt} \ge 0$ before the fourth step. In the third step, if the paths are planned using the method described in Case III, length l_s is increased to l_{s2} ($l_{s2} < l_{s3}$). As long as l_{s3} is within the stroke of B3-C3, l_{s2} is also within the stroke.

4.5 Design of path planner

Figure 12 shows the path generation process of the FSPP method. Based on this method, a path planner is developed. This planner has the following advantages:

1) The paths are planned using the basic movements shown in Fig. 4. The carts move with a uniform velocity, except for the motion of A2 in the third step. This simplifies the decentralized control system for the carts.
2) Only the initial and target poses of the platform need to be input into the planner. B3-C3 will never travel out of

[DOI: 10.1299/jamdsm.2023jamdsm0020]

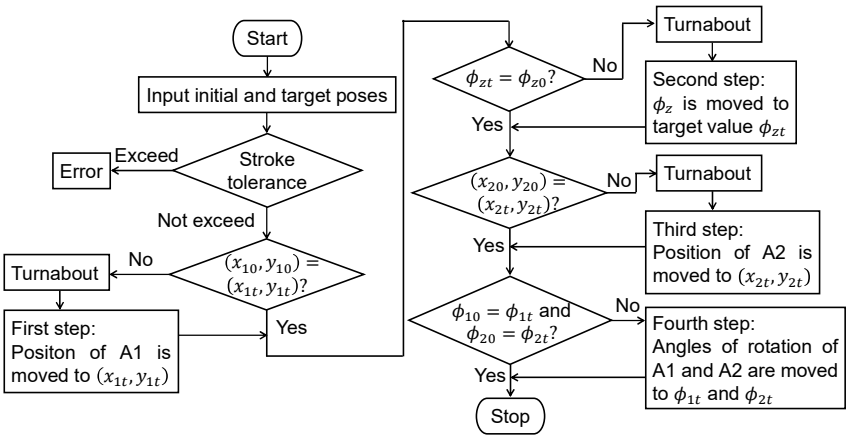

Fig. 12 Flow chart of FSPP method.

its stroke during the four steps as long as its initial and target screw displacements are within the stroke. Therefore, measurement devices for the movements of B3-C3, such as proximity sensors, are unnecessary.

3) B3 is rotated mainly in the fourth step. Thus, drastic changes in ϕ_y can be avoided in the first three steps.

In the next two sections, the performance of this planner is evaluated using simulations and experiments.

5. Simulation

The above kinematic analysis and path planning method were based on the rolling-without-slipping condition for carts A1 and A2 which is represented by Eq. (8). However, if the moving carts deviate from the specified paths due to small wheel slips, this deviation may accumulate during cart motion. Therefore, a feedback control strategy is needed for the carts to track the paths. Kinematics-based tracking control methods have been proposed for 2WD carts (Samson and Ait-Abderrahim, 1991; Sampei, et al., 1991). In this study, we employ an effective and easily realizable method proposed by Kanayama et al. (1990).

In this section, we perform simulations to verify the validity of the FSPP method and the tracking control strategy. The changes in the pose of the platform and the carts in each step are investigated.

5.1 Tracking control strategy

We utilize $\boldsymbol{p}_i = \{x_i, y_i, \phi_i\}^T$ and $\boldsymbol{p}_{a,i} = \{x_{a,i}, y_{a,i}, \phi_{a,i}\}^T$ to respectively represent the planned and actual poses of A1 and A2. If the carts deviate from the planned paths, the difference between $\boldsymbol{p}_i$ and $\boldsymbol{p}_{a,i}$ with respect to $O_{c,i}$–$X_{c,i}Y_{c,i}Z_{c,i}$ can be represented as follows:

$$\begin{Bmatrix} x_{e,i} \\ y_{e,i} \\ \phi_{e,i} \end{Bmatrix} = \begin{bmatrix} \cos\phi_{a,i} & \sin\phi_{a,i} & 0 \\ -\sin\phi_{a,i} & \cos\phi_{a,i} & 0 \\ 0 & 0 & 1 \end{bmatrix} (\boldsymbol{p}_i - \boldsymbol{p}_{a,i}), (i = 1, 2). \tag{27}$$

Following Kanayama et al. (1990), the actual translational and rotational velocity commands for the carts, i.e., $v_{c,i}$ and $\omega_{c,i}$, were obtained using the planned translational velocity v_i and rotational velocity ω_i as follows:

$$\begin{aligned} v_{c,i} &= v_i \cos\phi_{e,i} + K_x x_{e,i}, \\ \omega_{c,i} &= \begin{cases} \omega_i + v_i\left(K_y y_{e,i} + K_\phi \sin\phi_{e,i}\right), (\text{if } \ v_i \geq 0), \\ \omega_i + v_i\left(K_y y_{e,i} - K_\phi \sin\phi_{e,i}\right), (\text{if } \ v_i < 0), \end{cases} (i = 1, 2), \end{aligned} \tag{28}$$

where K_x, K_y, and K_ϕ are positive constants. They are set to $K_x = 1$ s^{-1}, $K_y = 25$ m^{-2}, and $K_\phi = 5$ m^{-1}. This control rule has been proven to be stable using Lyapunov stability theory (Kanayama, et al., 1990). By substituting $v_{c,i}$ and $\omega_{c,i}$ into the following equation, the rotational speeds of the left and right drive wheels of each cart, i.e., $\omega_{l,i}$ and

[DOI: 10.1299/jamdsm.2023jamdsm0020]

Table 2 Parameters for VEMOPAM.

Symbol	l_1	l_2	l_3	l_s	l_{scon}	z_{con}	p_1	p_2	r	w	v_0	ω_0
Value	42	150	71.5	266±95	266	542.5	20	160	62.5	99.5	75	0.38
Unit	mm	mm	mm	mm	mm	mm	mm/r	mm/r	mm	mm	mm/s	rad/s

Table 3 Initial and target poses of platform and carts.

	x [mm]	y [mm]	z [mm]	ϕ_x [rad]	ϕ_y [rad]	ϕ_z [rad]
Initial pose	0	0	542.5	0	0	0
First target pose	600	300	450	$\pi/4$	$-\pi/2$	$2\pi/3$
Second target pose	1200	600	500	$\pi/6$	$\pi/2$	$\pi/3$
	x_1 [mm]	y_1 [mm]	ϕ_1 [rad]	x_2 [mm]	y_2 [mm]	ϕ_2 [rad]
Initial pose	150	−113.5	0	−150	308	0
First target pose	605.2	476.2	15.0π	451.2	40.9	-11.7π
Second target pose	1365.0	677.9	8.2π	919.1	589.0	-6.7π

$\omega_{r,i}$, can be obtained:

$$\begin{Bmatrix} \omega_{l,i} \\ \omega_{r,i} \end{Bmatrix} = \frac{1}{r}\begin{bmatrix} 1 & -w \\ 1 & w \end{bmatrix} \begin{Bmatrix} v_{c,i} \\ \omega_{c,i} \end{Bmatrix}, (i = 1, 2), \tag{29}$$

where r is the radius of the drive wheel, and w is the distance between the CP of the cart and the touchdown point of the drive wheel (see Fig. 3). To make the carts smoothly track the paths, we apply a limiter to limit the maximum rotational speed of the drive wheels to 1.91π rad/s.

5.2 Simulation conditions and results

The parameters for VEMOPAM's model (see Fig. 3) used for the simulations are shown in Table 2. In the next section, we describe the experimental prototype of VEMOPAM with the same parameters and explain the design of these parameters in detail. Two sets of simulations, in which the initial and target poses of the platform and the carts are set as shown in Table 3, are performed. First, the platform is moved from the initial pose to the first target pose (first set). Then, it is moved from the first target pose to the second target pose (second set).

Under the above simulation conditions, the motions of A1 and A2 were planned by the FSPP method as shown in Fig. 13. The red dotted lines show the space necessary for the carts to move. As long as no obstacles exist in this space, the carts can reach the target positions. The poses of the carts were then simulated; the results of the simulations are shown in Fig. 14. The results in the ideal situation are indicated by solid lines and the target poses shown in Table II are indicated by black horizontal dotted lines. To demonstrate the effectiveness of the tracking control method, we

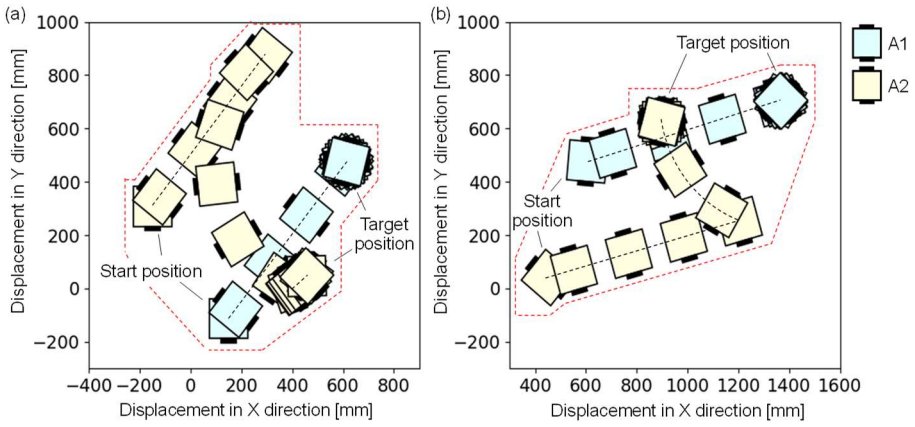

Fig. 13 Planned paths for simulations: (a) from initial pose to first target pose and (b) from first target pose to second target pose.

[DOI: 10.1299/jamdsm.2023jamdsm0020]

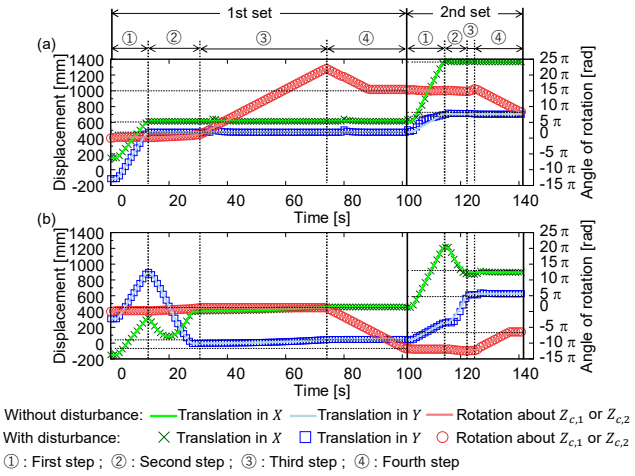

Fig. 14 Poses of (a) A1 and (b) A2 in four steps of path planning.

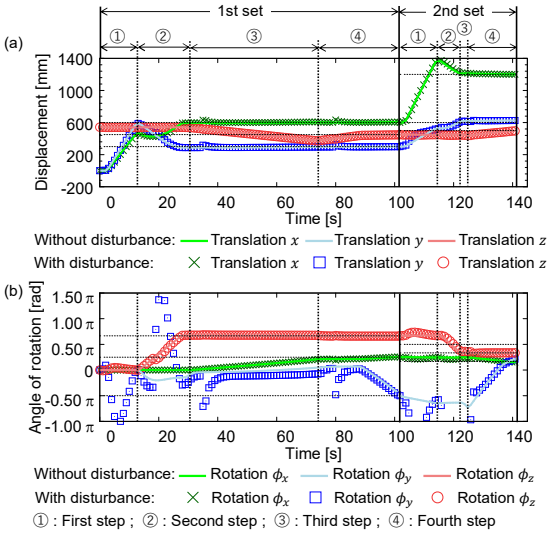

Fig. 15 Simulation results of (a) position and (b) orientation of platform in four steps of path planning.

simulated a situation in which the carts deviated due to disturbances. The disturbances acted on A1 at 35, 80, 101.8, and 115 s, and acted on A2 at 0, 18, 115, and 126 s. The disturbances all had the same magnitude. Figure 14 shows that the carts automatically tracked the planned paths even when they were disturbed, which verifies the validity of the tracking control strategy. The screw pairs did not exceed their strokes during the motion. These results verify the three advantages of the FSPP method shown in Section 4.5.

Changes in the pose of the platform in the four steps were also simulated; Figure 15 shows the results. As shown in this figure, with the tracking control method, the platform can be accurately moved to its first and second target poses. The changes in position (x, y, z), yaw ϕ_x, and roll ϕ_z of the platform caused by the disturbances were very small. However, the pitch ϕ_y drastically changed. This result indicates that the sensitivity of ϕ_y to external disturbances is significantly larger than those of the other five outputs, which agrees with the prediction in Section 2.3. In the next section, we discuss how to reduce the sensitivity of ϕ_y using a speed reduction mechanism.

6. Experiment

6.1 Development of prototype

We constructed a prototype of VEMOPAM (see Fig. 16). The specifications of this prototype are shown in Table 2. Regarding the design of these specifications, we first considered the specifications of the screw pairs (the strokes, leads, etc.), then determined the workspace of the platform, and finally designed the sizes of the other structures to guarantee that the size of the whole mechanism is small and that the two carts could avoid collision with each other. This prototype had two 2WD carts (A1 and A2) that were separately controlled. Each cart had a mini-computer and two motors. In this experiment, the load on the platform is its own weight.

Three ball screws were used as screw pairs B1-C1, B2-C2, and B3-C3. As shown in Table 2, B1-C1 and B2-C2 had the same stroke (450 mm) and lead (20 mm/r), and B3-C3 had a shorter stroke (190 mm) and a larger lead (160 mm/r). These strokes and leads guaranteed that ϕ_x could change within the range of $-\pi/2$ to $\pi/2$, and ϕ_y and ϕ_z could change within the range of $-\pi$ to π. However, most large-lead ball screws on the market are large and heavy, which adversely affects the stability of the mechanism. Therefore, we selected a ball screw with a lead of 20 mm/r as B3-C3 and developed a speed reducer, named the lead elongation mechanism (LEM), to increase the equivalent lead of B3-C3 to 160 mm/r. As shown in Fig. 16, the LEM had three pairs of timing pulleys and belts; the transmission ratio of each pair was 1:2. Screw shaft B3 was connected to the LEM via a radial bearing with a proper allowable thrust load. With this configuration, for every eight rotations of B3, one rotation was transmitted to the platform. Hence, a 1-mm error in the screw motion of B3-C3 results in a 2.25° error of ϕ_y, which is considered to be tolerable.

[DOI: 10.1299/jamdsm.2023jamdsm0020]

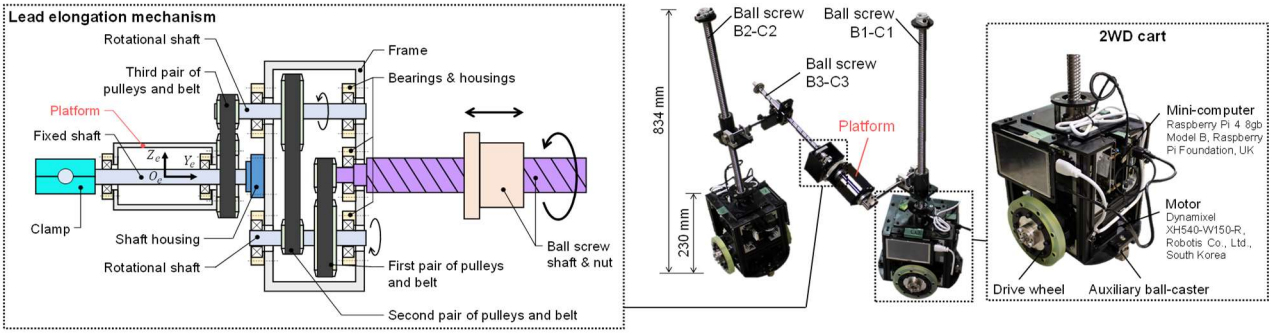

Fig. 16 Prototype of VEMOPAM, close-up view of 2WD cart, and structure of lead elongation mechanism (LEM).

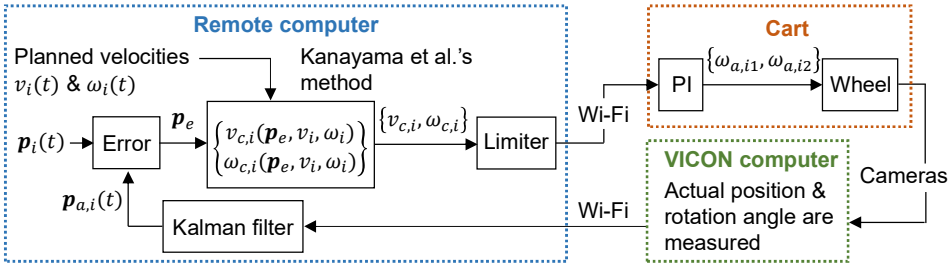

Fig. 17 Feedback tracking control system.

6.2 Feedback control system

Figure 17 shows the feedback control system for VEMOPAM. To measure the motions of the platform and the carts, six markers were fixed on the platform and three markers were fixed on the each of the carts. Six VICON motion capture cameras (VICON MX Bonita, Vicon Motion Systems Ltd., UK) surrounding VEMOPAM were used to measure the positions of the markers. The specifications for the cameras are given in Table 4. We used a computer with a VICON motion tracking application (VICON Tracker) installed to record and send the position information of the markers to a remote computer. A Kalman filter was used to eliminate inaccuracies and noise in the position information. Then, on the remote computer, the forward and rotation speed commands of the carts were determined using Kanayama's method (1990), as described in the previous section. These commands were sent from the remote computer to the mini-computers on the carts every 0.1 s. The speed commands of the drive wheels were then calculated and sent to the motors. To accurately output these speed commands, a proportional-integral (PI) controller for each motor was used (the gains were $K_P = 100$ and $K_I = 1920$). The computers communicated with each other over Wi-Fi. The commands from the remote computer were sent to A1 and A2 in simultaneous multithreading mode, which ensured that they started moving at precisely the same moment. Before the experiment, we conducted preliminary experiments to decide the parameters for the control system (e.g., the gains) and to confirm its stability.

6.3 Experimental results and discussion

Using the prototype, we conducted an experiment to assess the validity of the FSPP method. The initial and target poses of the platform were the same as those in the first set of the simulations (i.e., the initial and the first target poses given in Table 3). Figure 18 shows photographs of the carts during the experiment. As shown, the prototype worked as expected.

Figure 19 shows the poses of A1 and A2 in the experiment. With the feedback control system, the carts approximately tracked the planned paths, verifying the validity of the FSPP method. However, a deviation of 429.9°

Table 4 Specifications for VICON motion capture camera.

Frame rate	Maximum shutter time	Resolution
240 Hz	0.5 ms	0.3 megapixel [640×480]
System latency	Operating range	Focal length of lens
2 ms	12 m	4−12 mm

[DOI: 10.1299/jamdsm.2023jamdsm0020]

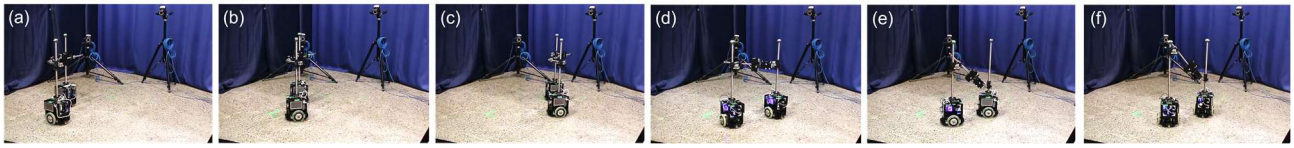

Fig. 18 Image sequence of carts during experiment. (a) Initial pose; (b) start of first step; (c) end of first step/start of second step; (d) end of second step/start of third step; (e) end of third step/start of fourth step; and (f) target pose.

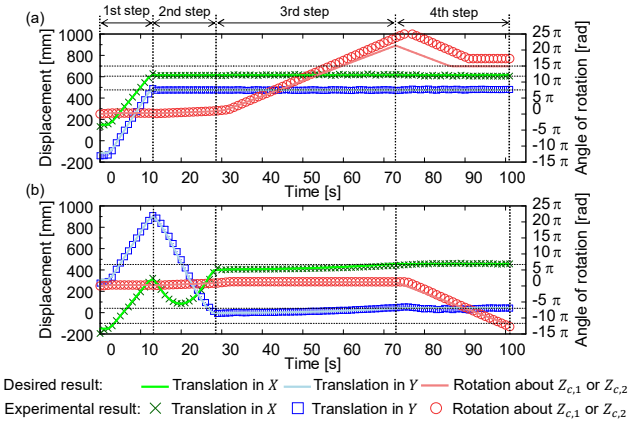

Fig. 19 Experimental results of poses of (a) A1 and (c) A2.

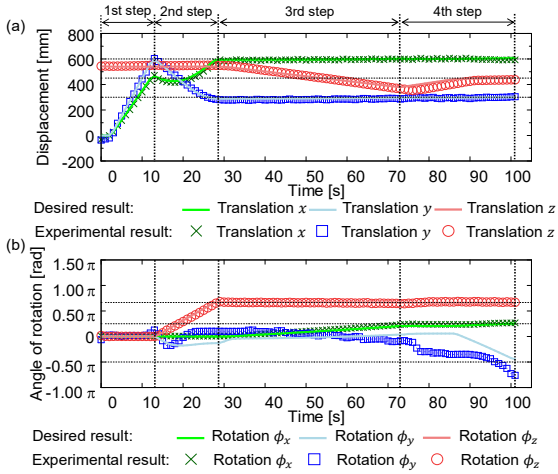

Fig. 20 Experimental results of (a) position and (b) orientation of platform.

occurred in the angle of rotation of A1 when the motion stopped. This might have occurred for the following reason. In the third step, due to the load from C1, A1 excessively rotated, which resulted in an error in the angles of rotation of the carts, i.e., $\phi_{e,i}$. The control rule represented by Eq. (28) indicates that when the carts were planned to be stopped in the fourth step (i.e., $v_i = \omega_i = 0$), $\phi_{e,i}$ could not be corrected in time because $\omega_{c,i} = 0$.

Figure 20 shows the pose of the platform in the experiment. We measured the errors between the desired pose and the actual pose every 0.1 s; the average errors are shown in Fig. 21. The error bars show the confidence interval at a 5% significance level. As shown in these figures, displacements x and y approximately reached their target values, whereas z deviated by 13.5 mm. The result of Welch's t-test demonstrates that the average error in z for the fourth step was significantly larger than those for the other steps, which is considered to have been caused by the deviation in the rotation of A1. Orientation angles ϕ_x and ϕ_z approximately reached their target values, whereas ϕ_y deviated by about 57.9° from the target value. The result of Welch's t-test shows that the average errors in ϕ_y were significantly larger than those of ϕ_x and ϕ_z for all four steps. This agrees with the prediction that ϕ_y has a high sensitivity. Welch's t-test also shows that the average error in ϕ_y for the fourth step is significantly larger than those for the other steps, as shown in Fig. 21(b). The reason for this is that ϕ_y was changed mainly in the fourth step, as planned.

Then, we discuss the possibility of improvement through the optimization of the design parameters. First of all, increasing the transmission ratio of the LEM can reduce the sensitivity of ϕ_y. For example, if we double the current transmission ratio to 1:16, the errors in ϕ_y can be theoretically reduced by 50%. However, in this case, with the current stroke of B3-C3 (190 mm), the movable range of ϕ_y becomes $-\pi/2$ to $\pi/2$. Conversely, to maintain the current movable range of ϕ_y, a stroke of the twice length is required. Thus, we should optimized the parameters

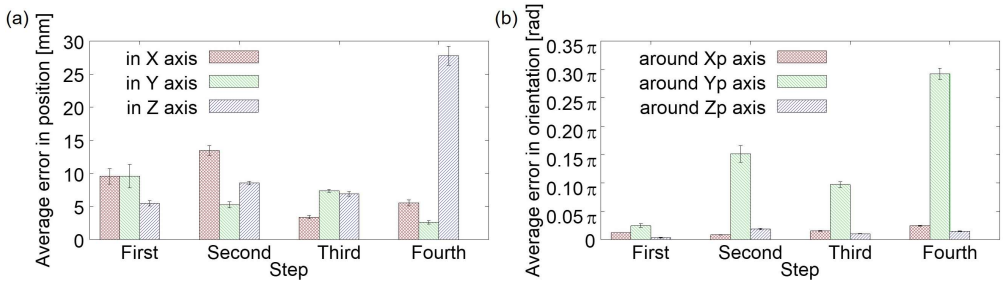

Fig. 21 Average errors in (a) position and (b) orientation of platform.

[DOI: 10.1299/jamdsm.2023jamdsm0020]

considering the error tolerance, movable range, and size of the robot. We can consider another approach to handle the error of ϕ_y. As described above, the errors in ϕ_y become significantly large in the fourth step. Thus, a robust control system for the rotations of the carts in this step would effectively reduce the errors in ϕ_y.

7. Conclusion

We proposed a novel MPM named VEMOPAM that consists of two 2WD carts and a parallel mechanism. The 6-DOF pose of the platform of VEMOPAM is controlled by the 2-DOF motions of the carts. Compared with conventional MPMs, VEMOPAM has fewer motors, which reduces the cost, weight, and size of the robots. We conducted a series of analyses and experiments and obtained analysis results as follows:

1) We described the structure of VEMOPAM and analyzed the inverse kinematics.
2) We proposed a path planning method for the two carts, and described the path generation in detail. This path planning method is also applicable for parallel mobile manipulators with other types of nonholonomic carts.
3) Simulations were conducted to investigate the motions of the platform. The simulation results confirmed that the platform reached the target pose as desired, and showed that its pitch ϕ_y is significantly sensitive to disturbances.
4) A prototype of VEMOPAM was developed for experiments. The experimental results showed that the pose, except for ϕ_y, of the platform approximately reached the target pose.

The prototype has two screw shafts (B1 and B2) unilaterally fixed on the carts. It can be used to assess the kinematic performance of VEMOPAM for low-speed motions. In the future, all the movable parts of this prototype could be mounted on one frame to improve vibration resistance, and the optimal design method for each part will be discussed. An obstacle avoidance method for the carts will be considered in future research. In addition, we will construct a dynamic model of VEMOPAM, analyze the changes of nonholonomic nature during the motion, and develop a robust control system especially to improve the control accuracy of ϕ_y.

Acknowledgment

The authors are grateful to T. Segoshi for his support.

References

AL-Taharwa, I., Sheta, A. and Al-Weshah, M., A mobile robot path planning using genetic algorithm in static environment, Journal of Computer Science, Vol.4, No.4 (2008), pp.341–344.

Arai, T., Analysis and synthesis of a parallel link manipulator based on its statics, Journal of the Robotics Society of Japan, Vol.10, No.4 (1992), pp.526–533 (in Japanese).

Arai, T., What is robot with integrated locomotion and manipulator, and its future?, Journal of the Robotics Society of Japan, Vol.13, No.7 (1995), pp.896–899 (in Japanese).

Ben-Horin, P., Djerassi, S., Shoham, M. and Ben-Horin, R., Dynamics of a six degrees-of-freedom parallel robot actuated by three two-wheel carts, Multibody Systems Dynamics, Vol.16, No.2 (2006), pp.105–121.

Ben-Horin, R., Shoham, M. and Djerassi, S., Kinetics, dynamics and construction of a planarly actuated parallel robot, Robotics and Computer-Integrated Manufacturing, Vol.14, No.2 (1998), pp.163–172.

Bischoff, R., Huggenberger, U. and Prassler, E., KUKA youBot - a mobile manipulator for research and education, 2011 IEEE International Conference on Robotics and Automation (2011).

Gosselin, C. and Angeles, J., Singularity analysis of closed-loop kinematic chains, IEEE Transactions on Robotics and Automation, Vol.6, No.3 (1990), pp.281–290.

Graf, R. and Dillmann, R., Acceleration compensation using a Stewart platform on a mobile robot, 1999 Third European Workshop on Advanced Mobile Robots. Proceedings (1999), pp.17–24.

Hashimoto, M., Oba, F. and Eguchi, T., Dynamic object-transportation control method by multiple mobile robots, Journal of the Robotics Society of Japan, Vol.13, No.6 (1995), pp.886–893 (in Japanese).

Jain, A. and Kemp, C. C., EL-E: an assistive mobile manipulator that autonomously fetches objects from flat surfaces, Autonomous Robots, Vol.28 (2009), pp.45–64.

[DOI: 10.1299/jamdsm.2023jamdsm0020]

Kanayama, Y., Kimura, Y., Miyazaki, F. and Noguchi, T., A stable tracking control method for an autonomous mobile robot, Proceedings., IEEE International Conference on Robotics and Automation (1990).

Koenig, S. and Likhachev, M., D* Lite, AAAI-02 Proceedings (2002), pp.476–483.

Kosuge, K., Oosumi, T. and Chiba, K., Decentralized control of multiple mobile robots handling a single object in coordination, Journal of the Robotics Society of Japan, Vol.16, No.1 (1998), pp.87–95 (in Japanese).

Kosuge, K., Oosumi, T. and Chiba, K., Load sharing of decentralized-controlled multiple mobile robots handling a single object, Proceedings of International Conference on Robotics and Automation (1997), pp.3373–3378.

Kosuge, K., Oosumi, T., Chiba, K. and Satou, M., Coordinated transportation by two nonholonomic mobile robots based on decentralized control, Transactions of the Japan Society of Mechanical Engineers Series C, Vol.65, No.634 (1999), pp.2379–2385 (in Japanese).

Lamini, C., Benhlima, S. and Elbekri, A., Genetic algorithm based approach for autonomous mobile robot path planning, Procedia Computer Science, Vol.127 (2018), pp.180–189.

Laumond, J. P., Jacobs, P. E., Taix, M. and Murray, R. M., A motion planner for nonholonomic mobile robots, IEEE Transactions on Robotics and Automation, Vol.10, No.5 (1994), pp.577–593.

Li, Y., Xu, Q. and Liu, Y., Novel design and modeling of a mobile parallel manipulator, Proceedings of the 2006 IEEE International Conference on Robotics and Automation (2006), pp.1135–1140.

Long, S., Terakawa, T. and Komori, M., Type synthesis of 6-DOF mobile parallel link mechanisms based on screw theory, Journal of Advanced Mechanical Design, Systems and Manufacturing, Vol.16, No.1 (2022), pp.JAMDSM0005.

Minami, M., Fujiwara, N. and Tsuge, H., Position and orientation control of manipulator mounted on autonomous mobile robot, Journal of the Robotics Society of Japan, Vol.11, No.1 (1993), pp.156–164 (in Japanese).

Moon, I., Miura, J. and Shirai, Y., Online viewpoint and motion planning method under uncertainty, Journal of the Robotics Society of Japan, Vol.17, No.8 (1999), pp.1107–1113 (in Japanese).

Sampei, M., Tamura, T., Itoh, T. and Nakamichi, M., Path tracking control of trailer-like mobile robot, Proceedings: IEEE/RSJ International Workshop on Intelligent Robots and Systems '91 (1991).

Samson, C. and Ait-Abderrahim, K., Feedback control of a nonholonomic wheeled cart in Cartesian space, Proceedings. 1991 IEEE International Conference on Robotics and Automation (1991).

Seki, H., Gao, Z., Kamiya, Y., Hikizu, M. and Zhang, Q., Trajectory generation of wheeled mobile robot by repeatedly direct kinematics, Journal of the Japan Society for Precision Engineering, Contributed Papers, Vol.71, No.4 (2005), pp.506–511 (in Japanese).

Shibata, T. and Fukuda, T., Path planning using Genetic Algorithm (2nd report, selfish planning and coordinative planning for multiple-mobile-robot systems), Transactions of the Japan Society of Mechanical Engineers Series C, Vol.59, No.560 (1993), pp.1134–1141 (in Japanese).

Shibata, T., Fukuda, T., Kosuge, K. and Arai, F., Path planning using Genetic Algorithm, Transactions of the Japan Society of Mechanical Engineers Series C, Vol.58, No.553 (1992), pp.120–126 (in Japanese).

Shoval, S. and Shoham, M., Sensory redundant parallel mobile mechanism, Proceedings 2001 IEEE International Conference on Robotics and Automation (2001), pp.2273–2278.

Stentz, A. and Hebert, M., A complete navigation system for goal acquisition in unknown environments, Autonomous Robots, Vol.2 (1995), pp.127–145.

Stentz, A., Optimal and efficient path planning for partially-known environments, Proceedings of the 1994 IEEE International Conference on Robotics and Automation (1994), pp.3310–3317.

Stewart, D., A platform with six degrees of freedom, Proceedings of the Institution of Mechanical Engineers, Vol.180, No.1 (1965), pp.371–386.

Terakawa, T., Komori, M. and Fujimoto, K., Control of an omnidirectional mobile robot with wheels connected by passive sliding joints, Journal of Advanced Mechanical Design, Systems, and Manufacturing, Vol.13, No.1 (2019), pp.JAMDSM0006.

Terakawa, T., Komori, M., Matsuda, K. and Mikami, S., A novel omnidirectional mobile robot with wheels connected by passive sliding joints, IEEE/ASME Transactions on Mechatronics, Vol.23, No.4 (2018), pp.1716–1727.

Tsai, L. W. and Tahmasebi, F., Synthesis and analysis of a new class of six-degree-of-freedom parallel minimanipulators, Journal of Robotic Systems, Vol.10, No.5 (1993), pp.561–580.

Tsubouchi, T., Naniwa, T. and Arimoto, S., Planning and navigation by a mobile robot in the presence of multiple

[DOI: 10.1299/jamdsm.2023jamdsm0020]

moving obstacles and their velocities, Journal of the Robotics Society of Japan, Vol.12, No.7 (1994), pp.1029–1037 (in Japanese).

Yamamoto, Y. and Yun, X., Coordinating locomotion and manipulation of a mobile manipulator, Proceedings of the 31st IEEE Conference on Decision and Control (1992), pp.2643–2648.

[DOI: 10.1299/jamdsm.2023jamdsm0020]